Check for updates

Energy Technology

Energy Technology
Generation, Conversion, Storage, Distribution

RESEARCH ARTICLE OPEN ACCESS

A Low Cost, Fully Sensorless Dual Axis PV Tracker Using Astronomical Ephemerides and Discrete Actuation

Khadidja Dahli[1] | Nawal Cheggaga[2] | Tayeb Allaoui[3] | Abdellah Benallal[4] | Adrian Ilinca[4]

[1]Automation Control Department, Faculty of Electrical Engineering, University of Science and Technology Houari Boumediene (USTHB), Algiers, Algeria | [2]Electrical and Remote Control Systems Laboratory (LabSET), Faculty of Technology, University of Saad Dahlab Blida 1, Blida, Algeria | [3]Electrical Engineering Department, Faculty of Science and Technology, University of Ibn Khaldoun, Tiaret, Algeria | [4]Department of Mechanical Engineering, École de Technologie Supérieure, Montreal, Quebec, Canada

Correspondence: Adrian Ilinca (adrian.ilinca@etsmtl.ca)

Received: 11 June 2026 | **Revised:** 21 September 2026 | **Accepted:** 14 October 2026

Keywords: dual-axis tracker | energy harvesting | low-cost automation | photovoltaic systems | renewable energy | sensorless control | solar tracking

ABSTRACT

Solar tracking systems can significantly increase photovoltaic (PV) energy production; however, conventional solutions often rely on sensors, feedback control systems, and continuous actuation, increasing cost, complexity, and maintenance requirements. This study presents a fully sensorless dual-axis solar tracking system that combines astronomical ephemerides with ZIP-code-based geographic localization to determine the optimal orientation of PV panels without optical, irradiance, GPS, or positioning sensors. The proposed approach employs discrete actuation to minimize mechanical movement and reduce energy consumption while maintaining high tracking accuracy. Simulation results, supported by experimental validation of the tracking mechanism, indicate that the proposed tracker increases daily energy output by approximately 56.65% compared with an equivalent fixed PV panel, while the energy consumed by the tracking mechanism represents only 1.17% of the additional energy generated. The analysis further demonstrates that tracking intervals between 1 and 2.5 h provide an effective compromise between energy production, actuator energy consumption, and mechanical wear. In addition, the system remains highly effective with tracking errors up to 12°, highlighting its robustness and suitability for low-cost implementations. The results show that a simple open-loop control architecture can substantially improve PV energy production with minimal hardware. The proposed sensorless tracking strategy therefore offers a practical, reliable, and cost-effective way to improve PV system performance, particularly in remote and resource-constrained regions.

1 | Introduction

The global photovoltaic (PV) sector has grown steadily over the past two decades, driven by declining technology costs, supportive energy policies, and rising demand for clean electricity. Global installed PV capacity has expanded rapidly, with average annual growth rates exceeding 40% during the early stages of market development, and solar energy is now among the most competitive sources of electricity worldwide [1–3]. Recent projections indicate that annual solar installations could approach or exceed 1 TW by the end of the decade, highlighting PV technology's central role in the global energy transition [4–7].

Countries with high solar irradiance are particularly well positioned to benefit from this expansion. Algeria has some of the world's most favorable solar resources and has set ambitious renewable energy targets, including deploying 22 GW of solar capacity by 2030 [8, 9]. Recent initiatives involving large-scale solar power plants and advanced PV technologies demonstrate the country's commitment to increasing solar energy's contribution to its national energy mix [10].

This is an open access article under the terms of the Creative Commons Attribution-NonCommercial-NoDerivs License, which permits use and distribution in any medium, provided the original work is properly cited, the use is non-commercial and no modifications or adaptations are made.

© 2026 The Author(s). *Energy Technology* published by Wiley-VCH GmbH.

Despite their growing deployment, fixed PV systems cannot fully exploit the available solar resource because the sun's apparent position changes continuously throughout the day and across seasons. Consequently, the angle of incidence between incoming solar radiation and the PV surface varies over time, reducing energy capture. Solar tracking systems mitigate this limitation by adjusting PV module orientation to follow the sun's trajectory, increasing energy yield by approximately 30% [11] to 40% [12] compared with fixed installations. Recent studies have reported gains of 35%–45% for dual-axis trackers and 20%–30% for single-axis systems in regions with high solar irradiance [13]. While continuous tracking can maximize energy production, it also increases actuator operation, energy consumption, and mechanical wear. Consequently, discrete and adaptive tracking strategies have recently attracted attention as effective ways to preserve most of the energy benefits of continuous tracking while reducing maintenance requirements and parasitic losses [14, 15].

Solar tracking technologies can generally be classified as sensor-based and sensorless approaches. Sensor-based systems rely on real-time feedback devices such as photodiodes, webcams, light-dependent resistors (LDRs), and other sensing technologies to align PV panels with the sun [16–19]. These systems have significantly improved energy production but may be sensitive to environmental conditions and often require calibration and maintenance.

Sensorless approaches seek to overcome these limitations using astronomical models, mathematical formulations, or optimization algorithms rather than direct irradiance measurements. Representative examples include systems based on differential evolution algorithms, sunrise and sunset data, predictable solar motion models, maximum power point tracking techniques, current-based optimization methods, and particle-filter algorithms [20–27]. Although these approaches eliminate many limitations associated with optical sensors, some still rely on auxiliary sensing devices or computationally intensive control strategies, which may increase implementation complexity and cost [28].

Despite considerable progress, several challenges remain. Sensor-based systems often require periodic calibration and may suffer performance degradation under adverse environmental conditions, while sensorless solutions frequently incorporate auxiliary sensors, complex optimization routines, or continuous tracking strategies that increase computational requirements, energy consumption, and mechanical wear [16–20, 23–26]. Furthermore, relatively few studies have investigated low-cost sensorless trackers under realistic operating conditions or evaluated the tradeoff between tracking accuracy, energy gain, actuator consumption, and mechanical complexity [29, 30]. Consequently, there remains a need for simple, robust, and economically attractive tracking systems capable of delivering substantial energy gains without extensive hardware requirements.

This work proposes a novel dual-axis solar tracking system designed to maximize net energy gain while maintaining low implementation cost and operational simplicity. The proposed approach relies exclusively on two inputs: the geographical coordinates of the installation site and astronomical algorithms used to determine the sun's position. Unlike many existing tracking systems, no optical sensors, GPS receivers, inclinometers, irradiance sensors, or feedback devices are required. The resulting architecture is therefore inherently robust, inexpensive, and easy to maintain.

A second key contribution lies in the adoption of a discrete event-driven tracking strategy. Rather than continuously adjusting panel orientation, the tracker operates at predetermined optimal intervals, thereby reducing actuator operating time, mechanical wear, and parasitic energy consumption. This approach is motivated by the observation that solar trackers can maintain nearly full tracking performance despite small angular deviations from the optimal position [31]. By combining precise astronomical positioning with intermittent actuation, the proposed system seeks to maximize practical energy gains while minimizing system complexity and operational losses. This philosophy aligns with recent calls for renewable energy technologies that prioritize reliability, affordability, and appropriate technological complexity, particularly for deployment in developing and emerging economies.

The remainder of this paper is structured as follows. Section 2 presents the proposed tracking strategy, system implementation, and performance evaluation methodology. Section 3 discusses the experimental results and compares the proposed approach with representative systems reported in the literature. Finally, Section 4 summarizes the main conclusions and outlines future research directions.

2 | Methods and Materials

2.1 | The Proposed Tracking Strategy

The proposed sensorless solar tracking system is designed to maximize PV energy capture using a simplified open-loop strategy. Operation begins with the user entering the installation site's postal code, allowing the system to identify the site's geographic coordinates. These coordinates, together with the current date and time, are then used in astronomical algorithms to calculate the sun's azimuth and elevation angles. Appendix A provides the detailed procedure for the Sun-position calculation.

The calculated solar angles were converted into actuator commands, allowing the tracker to orient the PV module toward the corresponding solar position. In the implemented prototype, the control algorithm can update the solar-position calculation at 15 min intervals. However, the actuation frequency is treated as an adjustable operating parameter since excessive movement may increase parasitic energy consumption and mechanical wear. The validated simulation model evaluates the influence of different tracking intervals, and the Results section discusses them to identify the best compromise between energy yield and actuator consumption.

By relying exclusively on geographic coordinates and astronomical models, the proposed tracker eliminates the need for optical, irradiance, GPS, or orientation sensors. It therefore operates as a true open-loop, no-feedback control system. Unlike sensor-based designs, its positioning strategy is not directly affected by temporary cloud cover, dust accumulation on sensors, or local

21944296, 2026, 11, Downloaded from https://onlinelibrary.wiley.com/doi/10.1002/ente.70709 by Ecole De Technologie Superieur, Wiley Online Library on [20/11/2026]. See the Terms and Conditions (https://onlinelibrary.wiley.com/terms-and-conditions) on Wiley Online Library for rules of use; OA articles are governed by the applicable Creative Commons License

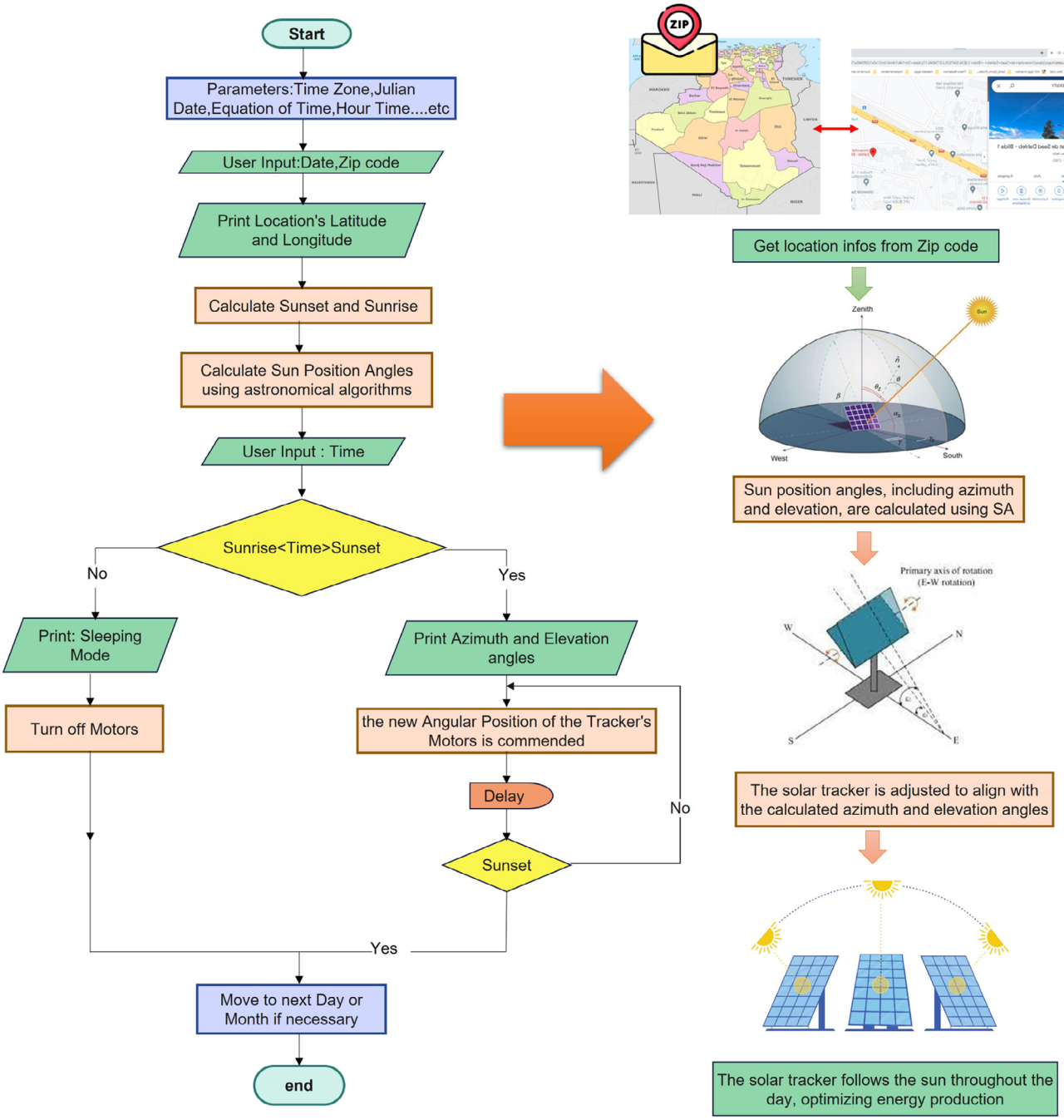


FIGURE 1 | Workflow of the proposed fully sensorless solar tracking strategy based on postal-code localization and astronomical sun-position calculation.

irradiance fluctuations. Moreover, discrete actuation limits unnecessary movements, reducing actuator energy consumption, mechanical wear, and vibration compared with continuously actuated or light-dependent resistor (LDR)-based tracking systems.

Postal-code-based localization also improves accessibility since users only need to provide a familiar postal-code-based location rather than manually entering latitude and longitude. This makes the approach suitable for deployment across regions with different geographic and climatic characteristics, while preserving a low-cost, user-friendly architecture.

The overall workflow of the proposed tracking strategy is illustrated in Figure 1.

2.2 | Geographic Data and ZIP Code Integration

The proposed tracking strategy determines the PV system's location using a postal code entered by the user. The postal code serves only as a convenient location identifier and is not used directly in the solar-position calculations. Instead, it serves as the key for retrieving the corresponding latitude and longitude coordinates from an embedded geographic database.

21944296, 2026, 11, Downloaded from https://onlinelibrary.wiley.com/doi/10.1002/ente.70799 by Ecole De Technologie Superieur, Wiley Online Library on [20/11/2026]. See the Terms and Conditions (https://onlinelibrary.wiley.com/terms-and-conditions) on Wiley Online Library for rules of use; OA articles are governed by the applicable Creative Commons License

The use of postal codes was inspired by location-based astronomical calculation systems commonly implemented in digital prayer watches, which determine prayer times and orientation from geographic coordinates and astronomical algorithms. Building on this concept, the proposed tracker replaces manual coordinate entry with a familiar postal-code interface, thereby simplifying system configuration while preserving positioning accuracy.

After the user enters the postal code, the microcontroller searches the embedded lookup database and retrieves the installation site's corresponding latitude and longitude. These geographic coordinates, together with the current date and time, constitute the actual inputs to the astronomical algorithm described in Appendix A. The algorithm then computes the solar azimuth and elevation angles required to orient the PV panel. Consequently, the postal code acts only as a geographic localization layer, whereas all solar-position calculations are performed exclusively using latitude, longitude, date, and time.

Unlike conventional tracking systems that determine geographic position using GPS receivers or other positioning devices, the proposed approach retrieves the required coordinates directly from the postal-code database. This eliminates the need for dedicated localization hardware while preserving the system's fully sensorless architecture and reducing both implementation cost and system complexity.

In this case study, the lookup database contains the postal codes and geographic coordinates of all administrative regions in Algeria. An excerpt of this database is presented in Table A1 in Appendix B. Although we experimentally validated the prototype using Algerian postal codes, the proposed methodology is not restricted to Algeria. The astronomical tracking algorithm is completely independent of the postal-code system. Deployment in another country only requires replacing or extending the lookup database with the corresponding postal codes (or any other geographic identifiers) and their associated latitude and longitude coordinates, while the remainder of the tracking algorithm remains unchanged.

This separation between the geographic localization layer and the astronomical tracking algorithm makes the proposed approach both scalable and easily transferable to other regions worldwide without modifying the underlying control strategy.

2.3 | Sun Position and Irradiance Calculations

The proposed tracking system determines the apparent position of the sun using established astronomical algorithms based on the geographic coordinates of the installation site, together with the date and time. The calculations provide two key parameters, namely, the solar azimuth and altitude angles, which are required for accurate panel orientation.

The solar azimuth angle represents the angular displacement of the Sun relative to a reference direction, typically true north. The solar altitude angle corresponds to the angular elevation of the sun above the horizon. Together, these two parameters define the apparent solar position in the sky and provide the information required to orient the PV module toward the incoming solar radiation.

For brevity, the detailed astronomical equations used to determine the solar azimuth and altitude angles are presented in Appendix A.

In addition to determining the solar position, the incident solar radiation on the tracking surface must be estimated in order to evaluate the potential energy gain associated with different panel orientations. The global irradiance received by a tilted surface is calculated by considering the beam, diffuse, and reflected radiation components.

The global irradiance incident on a tilted PV surface can be expressed as the sum of the beam, diffuse, and ground-reflected radiation components [32].

$$G_{T,\beta} = G_{B,\beta} + G_{D,\beta} + G_R \tag{1}$$

Which can be rewritten as:

$$G_{T,\beta} = G_B R_B + G_D R_D + G_T \rho R_R \tag{2}$$

where $G_{T,\beta}$ is the global irradiance on the tilted surface, G_B is the beam irradiance, G_D is the diffuse irradiance, G_T is the global horizontal irradiance, ρ is the ground reflectance, and R_B, R_D, and R_R are the geometric correction factors associated with beam, diffuse, and reflected radiation, respectively.

$$R_B = \frac{\cos(L-\beta)\cos(\delta)\sin(w_{ss})}{\cos(L)\cos(\delta)\sin(w_{ss}) + w_{ss}\sin(L)\sin(\delta)} + \frac{w_{ss}\sin(L-\beta)\sin(\delta)}{\cos(L)\cos(\delta)\sin(w_{ss}) + w_{ss}\sin(L)\sin(\delta)} \tag{3}$$

where w_{ss} denotes the sunset hour angle.

$$R_R = \frac{1-\cos(\beta)}{2} \tag{4}$$

$$R_D = \frac{1+\cos(\beta)}{2} \tag{5}$$

2.4 | Implementation of the Proposed System

2.4.1 | *Command Circuit*

The control architecture of the proposed solar tracker is based on an Arduino Mega microcontroller, which executes the solar-position algorithm and coordinates the tracking operations. Two stepper motors are employed to control the tracker orientation: a NEMA23 motor for azimuth motion and a NEMA17 motor for elevation adjustment. Motor actuation is achieved through dedicated driver modules, while a keypad and an LCD interface enable user interaction and system monitoring.

The user enters the postal code, along with the date and time information required for solar-position calculations. The entered postal code is matched with the corresponding entry

21944296, 2026, 11, Downloaded from https://onlinelibrary.wiley.com/doi/10.1002/ente.70709 by Ecole De Technologie Superieur, Wiley Online Library on [20/11/2026]. See the Terms and Conditions (https://onlinelibrary.wiley.com/terms-and-conditions) on Wiley Online Library for rules of use; OA articles are governed by the applicable Creative Commons License

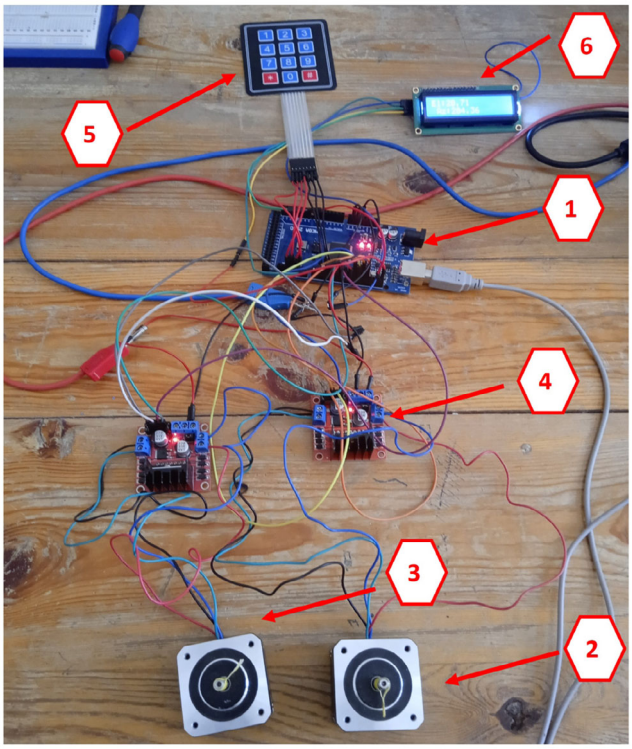


FIGURE 2 | The electrical components of the designed solar tracker system.

in the embedded database to retrieve the geographic coordinates of the installation site. The retrieved latitude and longitude are then converted to radians and used, together with the date and time, as inputs to the solar-position algorithm to determine the solar elevation and azimuth angles. Based on these calculated angles, the controller generates the corresponding motor commands. Figure 2 shows a photograph of the main electronic components.

The main components used in the electrical setup are summarized in Table 1. It includes essential details such as the model names, specifications, and estimated costs for each component. This table serves as a quick reference for readers, offering a clear overview of the key components utilized in our system design.

2.4.2 | Prototype

A laboratory-scale dual-axis solar tracker prototype was developed to validate the proposed tracking strategy. The mechanical structure was designed to provide adequate rigidity while maintaining low manufacturing cost and ease of assembly. Particular attention was given to tracking precision, structural stability, and operational reliability under outdoor conditions.

The tracker employs two independent actuation systems. Elevation tracking is achieved using a lead-screw linear actuator driven by a NEMA17 stepper motor, whereas azimuth tracking is performed through a belt-driven mechanism actuated by a NEMA23 stepper motor. This configuration enables independent control of both rotational axes while maintaining a simple and cost-effective mechanical architecture. The three-dimensional model of the proposed system is shown in Figure 3.

The decision to use a linear screw actuator for elevation tracking was based on the need for precision and its ability to handle moderate loads effectively. Meanwhile, the choice of a belt drive system for azimuth tracking was driven by its smooth motion and cost-effectiveness, as azimuth angle adjustments typically require lower precision. These component selections were carefully made to optimize the performance and cost-effectiveness of the solar tracking system for its specific purposes.

TABLE 1 | Main specifications and estimated costs of components used in the electrical setup.

N°	Component	Model	Specifications	Cost
1	Arduino board	Arduino mega 2560	– Microcontroller: ATmega 2560 – Digital I/O pins: 54 – Flash memory: 256 – Communication interfaces: 4 UART serial communication ports	4700 DA
2	NEMA23 Stepper motor	1m-57HS76-3004	– Step angle: 1.8° – Holding torque: 4 Ncm – Current rating: 1.68 A	6500 DA
3	NEMA17 Stepper motor	1m-42HS34-1334AC	– Step angle: 1.8° – Holding torque: 26 Ncm – Current rating: 0.4 A	2900 DA
4	LN298N motor driver	LN298N	– Maximum motor voltage: 46 V – Maximum continuous current: 2 A – Motor control type: the dual H-bridge driver	1200 DA
5	Keypad	3 × 4 keypad	– Number of keys: 12 – Keypad output: digital – Keypad interface: serial or parallel	900 DA
6	LCD display	16 × 2 I2C LCD display	– Display size: 16 characters × 2 lines – Interface: I2C	1300 DA

21944296, 2026, 11, Downloaded from https://onlinelibrary.wiley.com/doi/10.1002/ente.70709 by Ecole De Technologie Superieur, Wiley Online Library on [20/11/2026]. See the Terms and Conditions (https://onlinelibrary.wiley.com/terms-and-conditions) on Wiley Online Library for rules of use; OA articles are governed by the applicable Creative Commons License

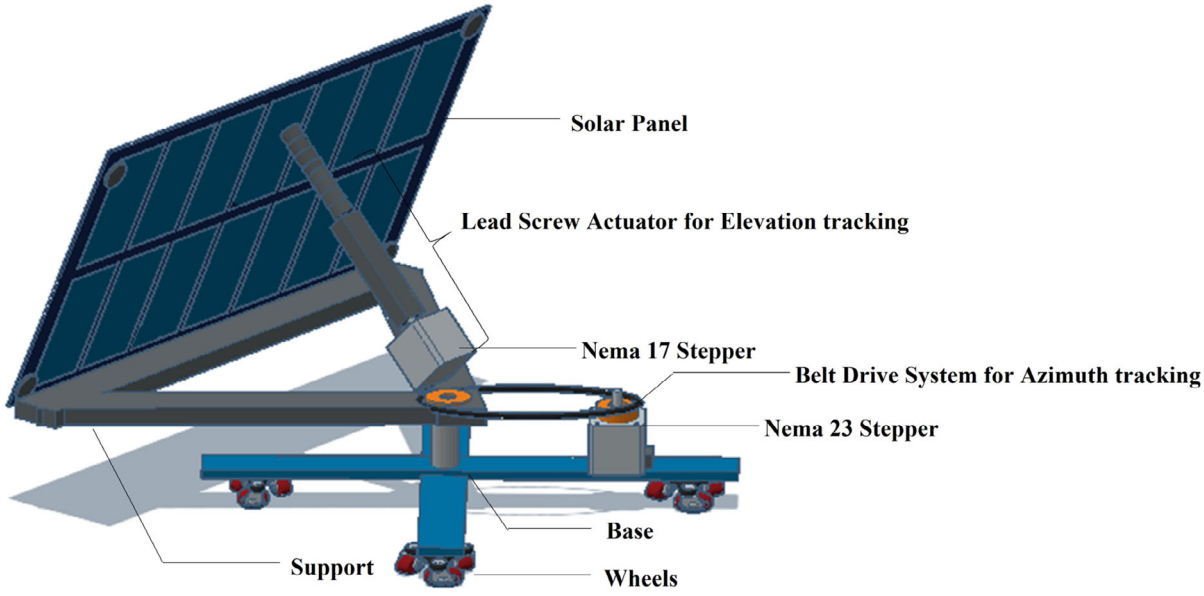


FIGURE 3 | 3D design of the sensor-less dual axes solar tracker with labels.

2.4.2.1 | *Azimuth Rotation Drive System.* The azimuth drive system uses a belt transmission mechanism that provides smooth rotation and mechanical reduction, improving angular resolution and positioning accuracy. The motor and transmission system were sized to meet the torque requirements for rotating the PV module (Figure 4).

The labeled components (1–6) represent key elements of the azimuth rotation drive system: Nema 23 stepper motor (1), drive pulley (2), V-type belt (3), driven pulley (4), support for the motor (5), and rotation axes for the driven system (6).

2.4.2.2 | *Elevation Rotation Drive System.* The elevation drive uses a lead-screw linear actuator to convert motor rotation into controlled linear displacement. This mechanism provides accurate tilt adjustment while ensuring sufficient mechanical advantage to support the PV module throughout the tracking range (Figure 5).

The numbered elements (1–4) provide a detailed breakdown of the components of the elevation drive system: support for the motor (1), Nema 17 stepper motor (2), nut (3), and screw (4).

The torque requirements of the azimuth and elevation drives were estimated to be approximately 0.2 and 1.1 N·m, respectively. Based on these requirements, NEMA23 and NEMA17 stepper motors were selected for the azimuth and elevation axes.

Utilizing a combination of a belt drive system and a linear actuator powered by stepper motors offers several advantages. It eliminates the need for a separate brake system or torque reducer, resulting in substantial cost savings and streamlining the solar tracker design. Additionally, this setup introduces no extra expenses or maintenance complications. Figure 6 shows the fully assembled mechanical components of the solar tracker with the PV module STP050D-12/MEA.

The experimental prototype was developed primarily to validate the proposed tracking strategy and verify the mechanical positioning of the PV panel under real operating conditions. The PV module mounted on the prototype was therefore used to confirm the correct tracking behavior. The electrical power and energy-performance results presented in Section 3 were not obtained from direct electrical measurements of the prototype. Instead, they came from the validated simulation model,

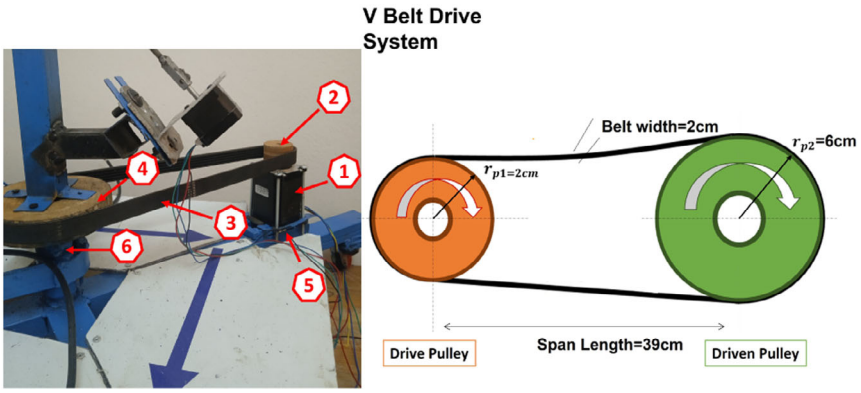


FIGURE 4 | Azimuth rotation drive system.

21944296, 2026, 11, Downloaded from https://onlinelibrary.wiley.com/doi/10.1002/ente.70709 by Ecole De Technologie Superieur, Wiley Online Library on [20/11/2026]. See the Terms and Conditions (https://onlinelibrary.wiley.com/terms-and-conditions) on Wiley Online Library for rules of use; OA articles are governed by the applicable Creative Commons License

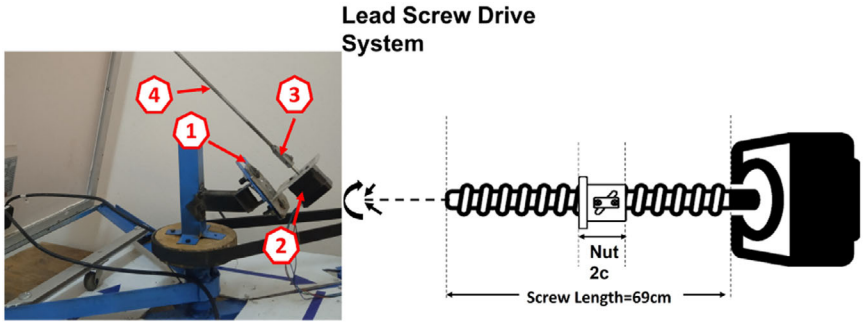


FIGURE 5 | Elevation rotation drive system.

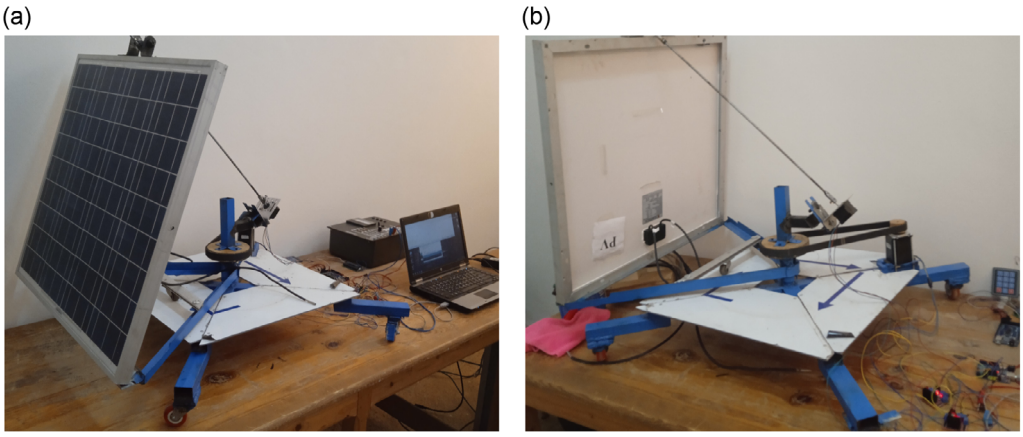


FIGURE 6 | The designed sensor-less dual axes solar tracker.

parameterized using the characteristics of the developed tracker, the PV module, and the tracking motors.

2.5 | Performance Evaluation Metrics

To evaluate the effectiveness of the proposed solar tracking strategy, we considered several performance indicators. These metrics quantify the energy benefit obtained through solar tracking while accounting for the energy consumed by the tracking mechanism itself. Because the primary purpose of the experimental prototype was to validate the tracking mechanism, we obtained the PV electrical performance indicators reported in this study from a validated simulation model parameterized with the actual characteristics of the developed tracker and PV module. We experimentally tested the physical prototype to verify its tracking response, orientation according to the calculated solar position, and mechanical stability.

The total electrical energy generated by the fixed PV panel during the test period is denoted by:

$$E_{\text{fixed}} = \sum_{i=1}^{N} P_{\text{fixed},i} \Delta t \tag{6}$$

where $P_{\text{fixed},i}$ is the instantaneous power produced by the fixed panel and Δt is the sampling interval.

Similarly, the electrical energy generated by the tracking system is calculated as:

$$E_{\text{tracker}} = \sum_{i=1}^{N} P_{\text{tracker},i} \Delta t \tag{7}$$

where $P_{\text{tracker},i}$ represents the instantaneous power generated by the tracked PV panel.

The electrical energy consumed by the tracking mechanism is determined as:

$$E_{\text{cons}} = \sum_{i=1}^{N} P_{\text{motor},i} \Delta t \tag{8}$$

where $P_{\text{motor},i}$ denotes the power required by the tracking motors and control electronics.

The net energy gain provided by the solar tracker is defined as

$$E_{\text{net}} = E_{\text{tracker}} - E_{\text{fixed}} - E_{\text{cons}} \tag{9}$$

The percentage energy improvement relative to the fixed system is then expressed as

$$G_E = \frac{E_{\text{net}}}{E_{\text{fixed}}} \times 100\% \tag{10}$$

21944296, 2026, 11, Downloaded from https://onlinelibrary.wiley.com/doi/10.1002/ente.70799 by Ecole De Technologie Superieur, Wiley Online Library on [20/11/2026]. See the Terms and Conditions (https://onlinelibrary.wiley.com/terms-and-conditions) on Wiley Online Library for rules of use; OA articles are governed by the applicable Creative Commons License

To assess tracking accuracy, the instantaneous tracking error is defined as:

$$\varepsilon = \sqrt{\left(\theta_{az} - \theta_{az}^{ref}\right)^2 + \left(\theta_{el} - \theta_{el}^{ref}\right)^2} \quad (11)$$

where θ_{az}^{ref} and θ_{el}^{ref} are the reference azimuth and elevation angles obtained from the astronomical model, while θ_{az} and θ_{el} correspond to the actual tracker orientation.

The mean tracking error over the entire experimental period is calculated as:

$$\bar{\varepsilon} = \frac{1}{N}\sum_{i=1}^{N} \varepsilon_i \quad (12)$$

3 | Experimental Validation and Performance Evaluation

3.1 | Experimental Validation and Simulation Framework

We evaluated the proposed solar tracking system using two complementary methodologies for different purposes. First, we constructed and experimentally tested a laboratory prototype under outdoor conditions to validate the tracking strategy, verify the calculated solar positions, and assess the mechanical operation of the dual-axis tracking mechanism. Second, the PV electrical performance of the system, including irradiance, power production, energy generation, and net energy gain, was evaluated using a validated simulation model parameterized with the characteristics of the developed tracker and PV module. Consequently, the experimental and simulation components of this study should be regarded as complementary rather than redundant.

Outdoor experiments were conducted in Tiaret, Algeria, between January 2022 and January 2023 to verify the tracking mechanism's robustness and accuracy under real environmental conditions. The PV module mounted on the prototype confirmed the tracker's correct orientation throughout the day rather than performing a complete electrical performance characterization.

The numerical simulations evaluated the electrical performance of the proposed tracking strategy under different geographic locations, seasonal conditions, tracking intervals, and tracking errors. Using the validated tracking algorithm and the characteristics of the developed prototype, the simulation model calculated the PV power production and the associated energy-performance indicators presented in Section 3. This combined methodology provides both experimental verification of the proposed tracking concept and quantitative evaluation of its expected energy performance.

3.2 | Comparative Study

To quantify the benefits of the proposed tracking strategy, we compared the developed solar tracker with an identical fixed PV panel operating under the same environmental conditions. The comparison focused on incident solar irradiance, output power, total energy production, and net energy gain after accounting for tracker energy consumption. Unless otherwise stated, this section reports power and energy values from the validated simulation model described in Section 3.1.

Figure 7 presents the simulated solar irradiance collected by the proposed tracker and the equivalent fixed PV panel. The average

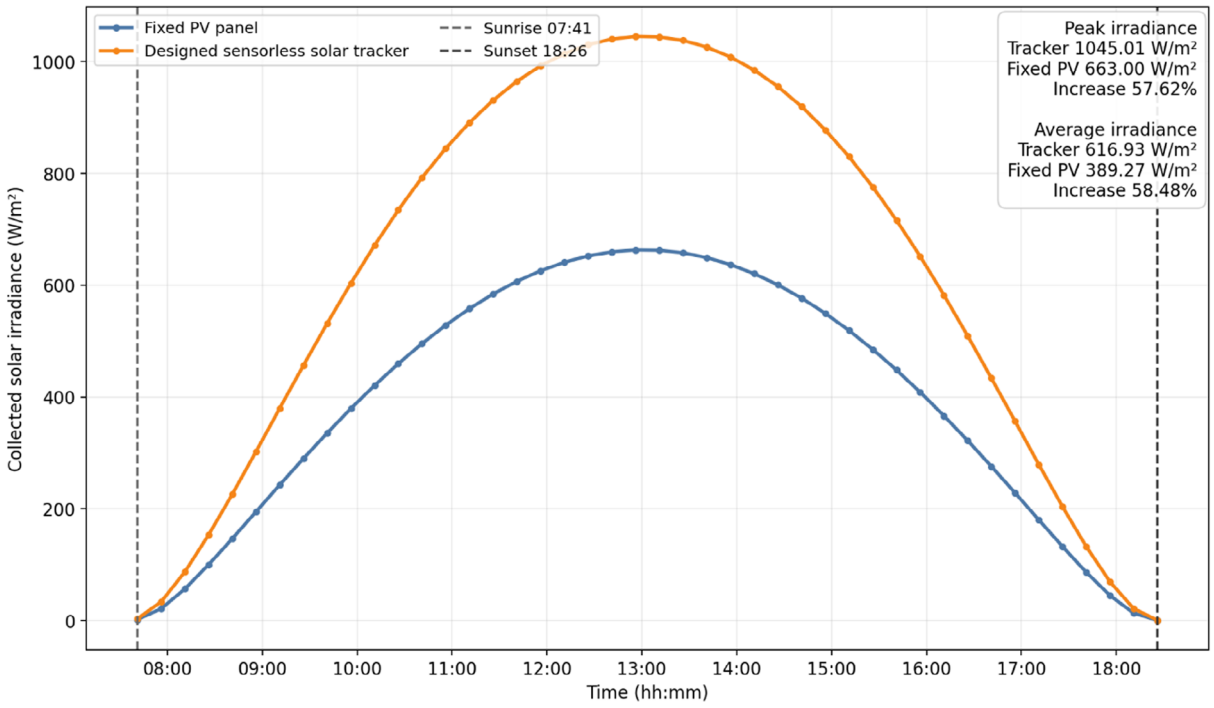


FIGURE 7 | Collected solar irradiance comparison between the designed sensorless solar tracker and a fixed PV panel.

21944296, 2026, 11, Downloaded from https://onlinelibrary.wiley.com/doi/10.1002/ente.70709 by Ecole De Technologie Superieur, Wiley Online Library on [20/11/2026]. See the Terms and Conditions (https://onlinelibrary.wiley.com/terms-and-conditions) on Wiley Online Library for rules of use; OA articles are governed by the applicable Creative Commons License

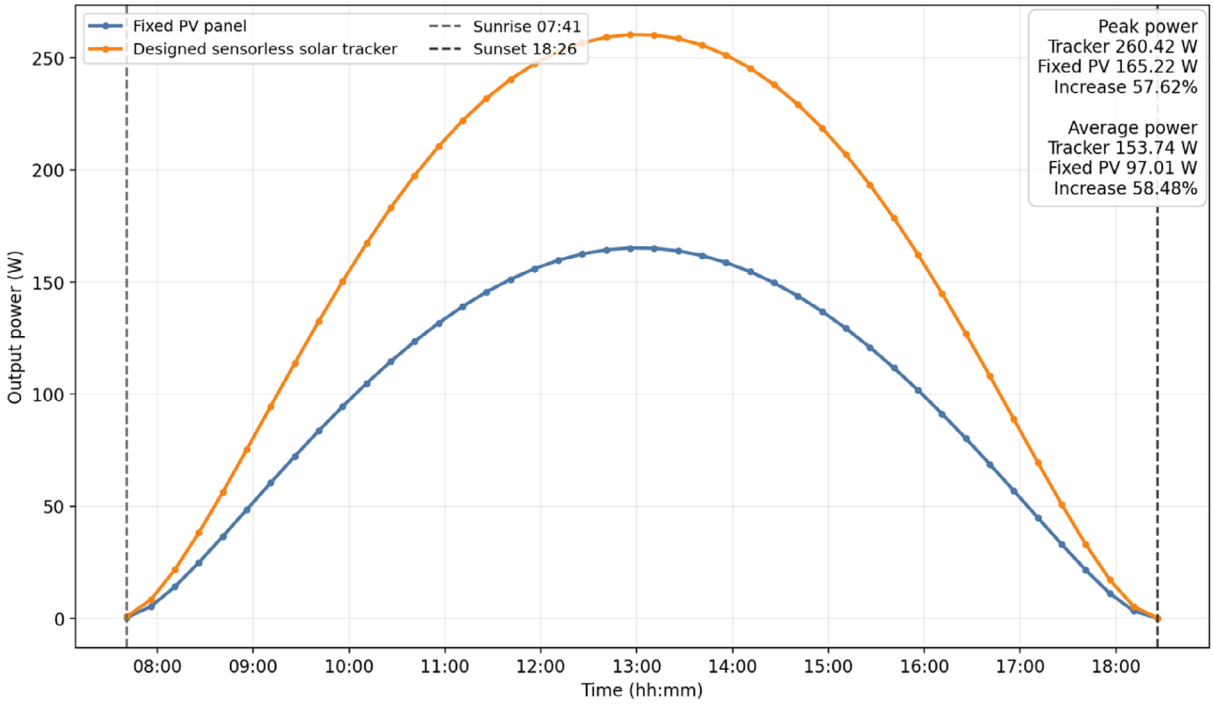


FIGURE 8 | Output power comparison of the designed solar tracker versus the fixed PV panel.

irradiance gain exceeded 58%, with the largest improvements occurring in the morning and afternoon, when fixed installations experience larger incidence-angle losses. These results confirm that the proposed tracking strategy maintains favorable panel orientation throughout the solar trajectory.

The increase in collected irradiance directly translates into higher electrical power output, as illustrated in Figure 8. The tracker maintains elevated power production during the entire daylight period, particularly during off-peak solar hours when fixed panels operate under less favorable incidence angles. Consequently, the proposed system achieves substantially greater daily energy production without requiring any irradiance or optical sensors.

The cumulative effect of improved irradiance capture and sustained power production is reflected in the daily energy yield. The tracking system generated approximately 1691 Wh compared with 1067 Wh for the fixed panel, corresponding to an increase of nearly 59%. Such gains are consistent with the upper range of improvements reported for dual-axis tracking systems in the literature and demonstrate the effectiveness of the proposed sensorless strategy.

After accounting for the energy required by the tracking mechanism, the proposed system achieved a net energy gain of 56.65% relative to the fixed configuration (Figure 9). The tracker energy consumption accounted for only 1.17% of the additional energy generated, showing that the benefits of tracking largely outweigh the associated actuation costs. These findings validate the central premise of this work: a fully sensorless architecture can achieve significant energy gains while maintaining negligible operational energy consumption.

3.3 | Optimal Tracking Time

We assessed the performance of a discretely actuated, sensorless solar tracking system over tracking intervals ranging from 15 min to 5 h. Figure 10 shows absolute energy values, while Figure 11 shows the corresponding normalized metrics.

As shown in Figure 10, generated energy decreases from about 1685 Wh at a 15 min interval to about 1640 Wh at a 5 h interval. Concurrently, actuation energy consumption decreases from about 1675 Wh at 15 min to nearly 1610 Wh at 5 h, highlighting the pronounced influence of tracking frequency on actuator energy losses.

When expressed in normalized terms (Figure 11), the consumed energy declines from 1.43% of generated energy at a 15 min interval to 0.36% at a 1 h interval, further reducing to below 0.2% for tracking intervals between 2 and 2.5 h and reaching as low as 0.07% at 5 h. Throughout this range, the normalized produced energy remains consistently high, exceeding 99.8% for intervals up to 2.5 h, but gradually decreases for longer intervals due to increased solar misalignment.

Evaluating the system solely on the basis of maximum net energy gain suggests that a 1 h tracking interval yields the optimal performance, with the highest net gain of approximately 99.88%. However, when the design criteria prioritize minimizing energy consumption to below 0.2% while sustaining energy production above 99.8%, the 2–2.5 h tracking interval emerges as the most favorable operating range. This interval offers an enhanced balance among actuation losses, energy yield, and mechanical activity for the proposed sensorless tracking system.

21944296, 2026, 11, Downloaded from https://onlinelibrary.wiley.com/doi/10.1002/ente.70709 by Ecole De Technologie Superieur, Wiley Online Library on [20/11/2026]. See the Terms and Conditions (https://onlinelibrary.wiley.com/terms-and-conditions) on Wiley Online Library for rules of use; OA articles are governed by the applicable Creative Commons License

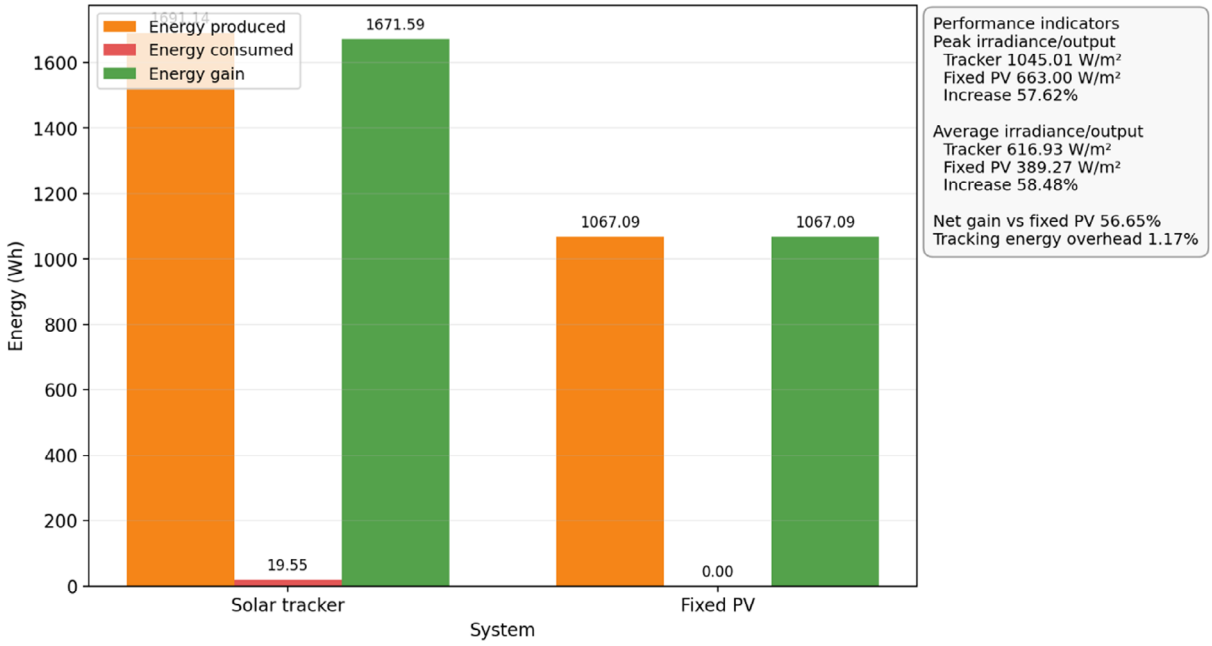


FIGURE 9 | Total energy generation and energy balance comparison between the solar tracker and the fixed PV system.

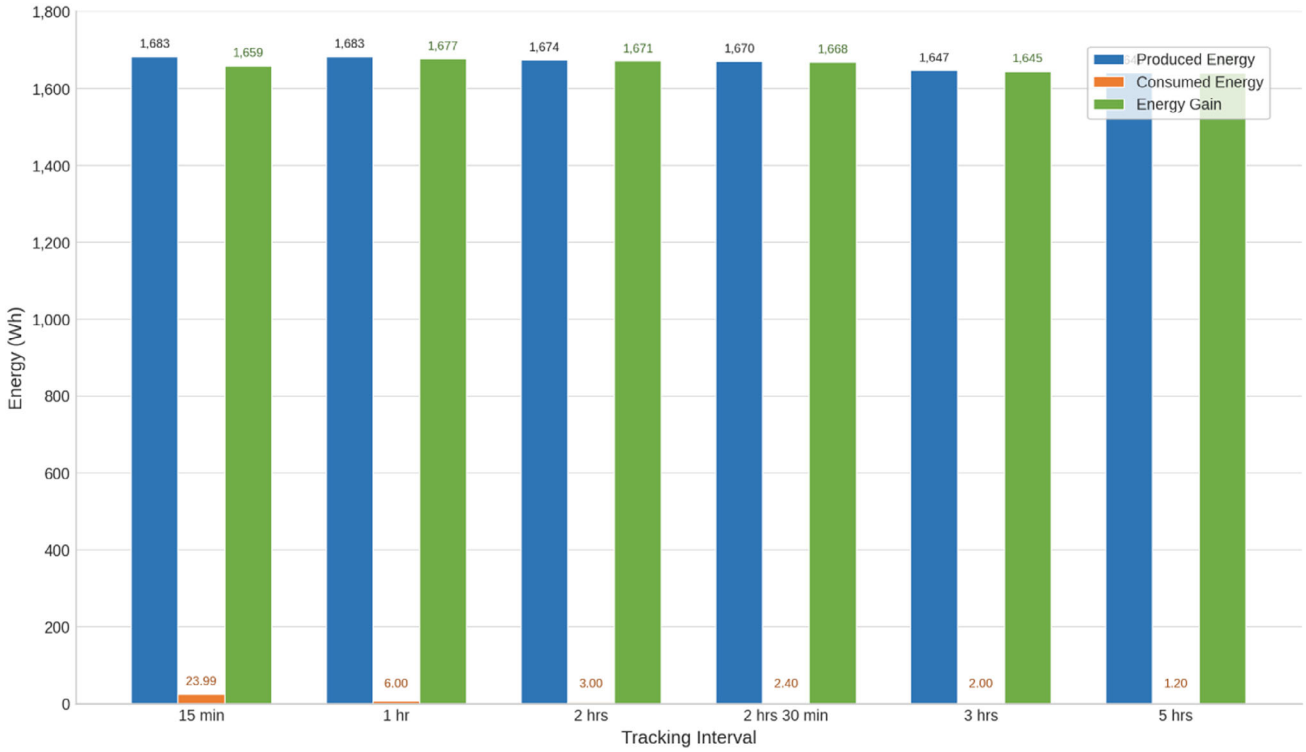


FIGURE 10 | Absolute produced energy, energy consumption, and net energy gain as a function of tracking interval for the proposed solar tracking system.

The results indicate that increasing tracking frequency beyond hourly operation provides only marginal gains in collected energy while significantly increasing actuation energy consumption. Consequently, discrete tracking represents a more attractive solution than continuous tracking for low-cost solar tracking systems.

3.4 | Tracking Error Impact on Solar Tracker Performance

We examined the influence of tracking error on the performance of a discretely actuated, sensorless solar tracker by introducing angular deviations ranging from 1° to 24°. Figures 12 and 13

21944296, 2026, 11, Downloaded from https://onlinelibrary.wiley.com/doi/10.1002/ente.70799 by Ecole De Technologie Superieur, Wiley Online Library on [20/11/2026]. See the Terms and Conditions (https://onlinelibrary.wiley.com/terms-and-conditions) on Wiley Online Library for rules of use; OA articles are governed by the applicable Creative Commons License

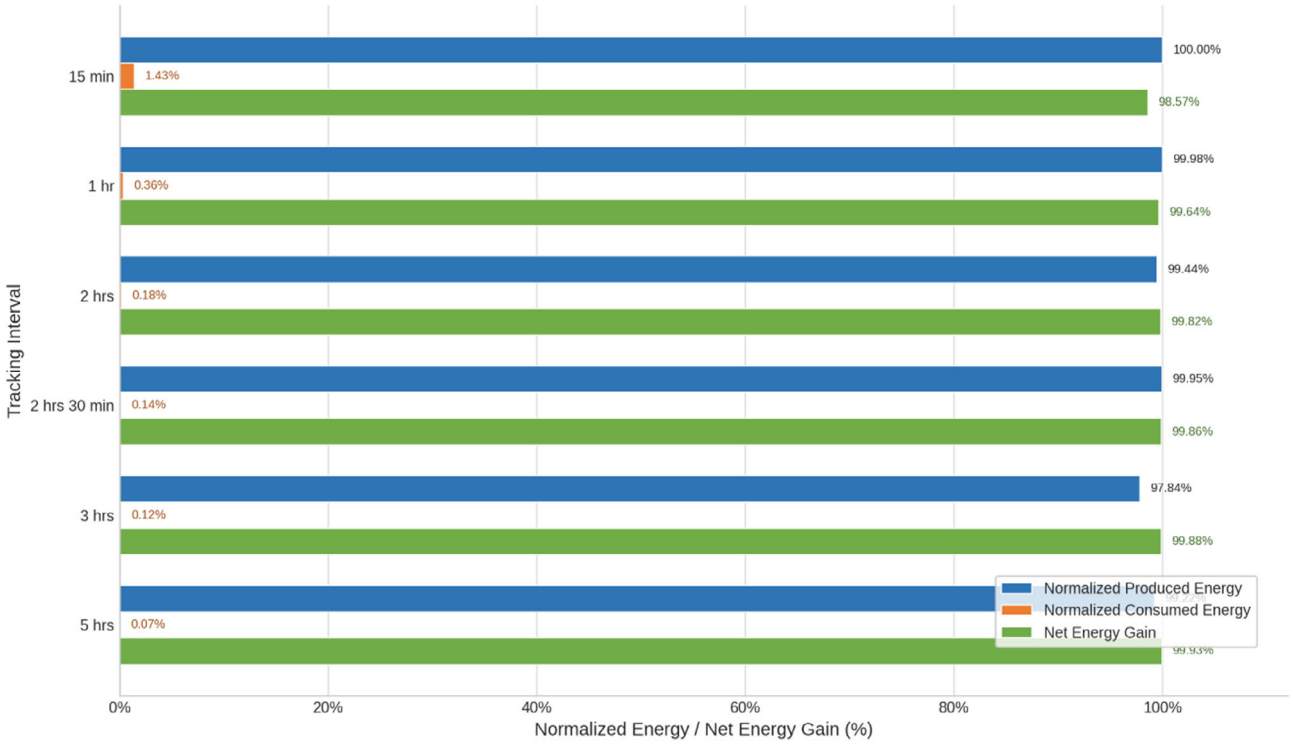


FIGURE 11 | Normalized produced energy, consumed energy, and net energy gain of the discretely actuated sensorless solar tracker under different tracking intervals.

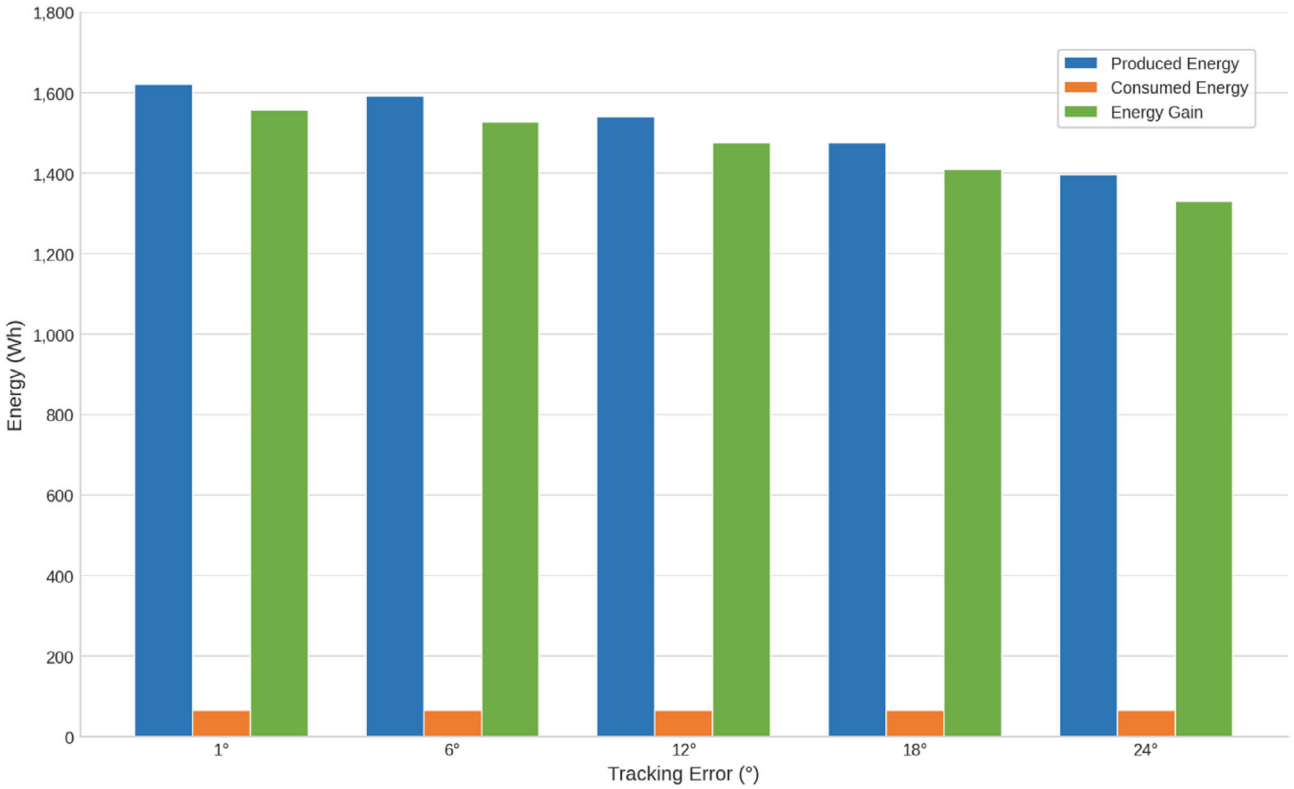


FIGURE 12 | Absolute produced energy, consumed energy, and net energy gain of the solar tracker under different tracking error angles.

present the corresponding absolute and normalized energy outputs, respectively.

As shown in Figure 12, the generated energy remains relatively stable for tracking errors up to 12°, decreasing slightly from about 1600 Wh at 1° to about 1550 Wh at 12°, indicating strong tolerance to moderate misalignment. Within this range, energy consumption remains low and nearly constant, resulting in a substantial net energy gain. However, when the tracking error exceeds 12°, performance declines markedly, with energy

21944296, 2026, 11, Downloaded from https://onlinelibrary.wiley.com/doi/10.1002/ente.70799 by Ecole De Technologie Superieur, Wiley Online Library on [20/11/2026]. See the Terms and Conditions (https://onlinelibrary.wiley.com/terms-and-conditions) on Wiley Online Library for rules of use; OA articles are governed by the applicable Creative Commons License

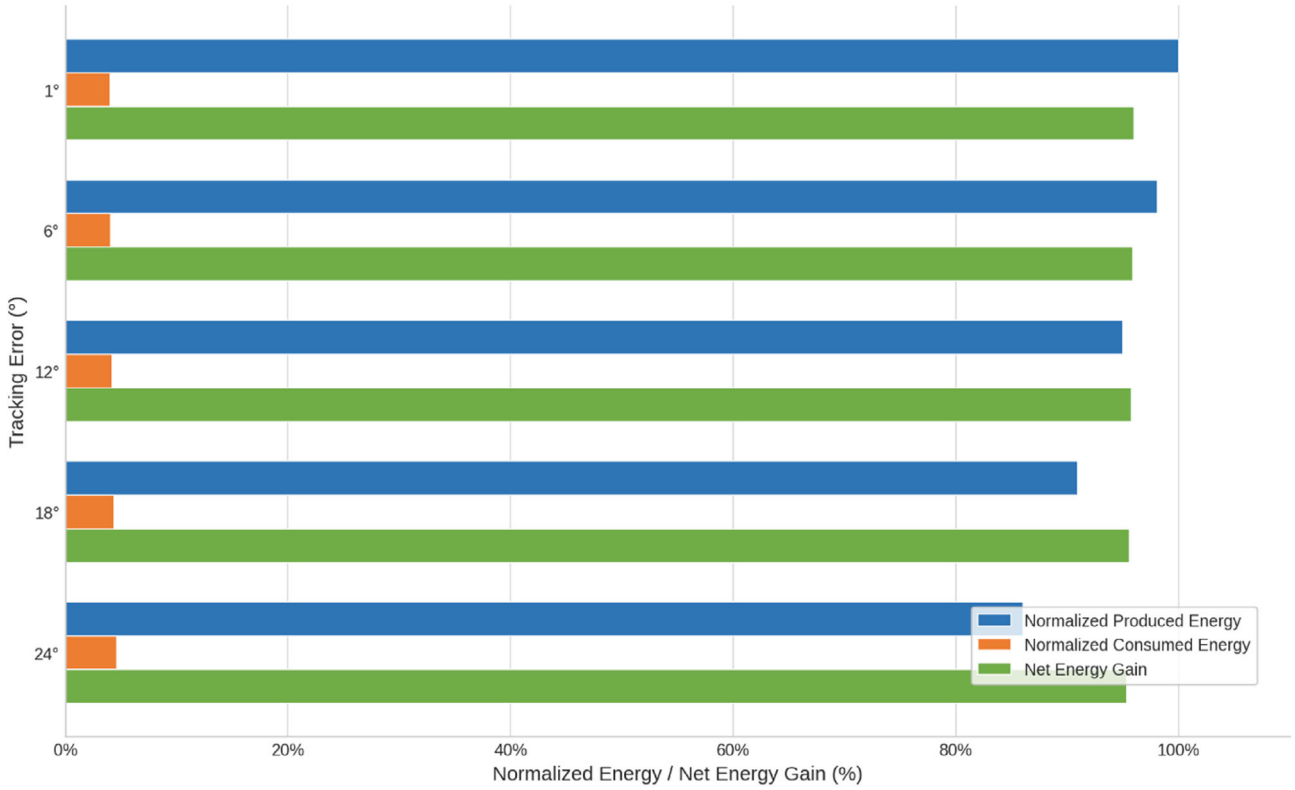


FIGURE 13 | Normalized produced energy, normalized consumed energy, and net energy gain as a function of tracking error.

production dropping to about 1450 Wh at 18° and further to about 1380 Wh at 24°, reflecting a greater loss of effective solar irradiance.

This pattern is more distinctly illustrated in the normalized energy results shown in Figure 13, where energy output remains near its maximum (net energy gain of 96%) for small angular deviations but progressively diminishes as the error increases. Despite this reduction, the tracker sustains a relatively high normalized energy gain even at moderate errors, demonstrating robustness against typical mechanical and environmental inaccuracies.

In summary, the findings indicate that tracking errors up to 12° exert minimal influence on system performance, whereas larger errors substantially reduce energy yield, underscoring the importance of maintaining reasonable alignment accuracy without necessitating highly precise or energy-intensive tracking mechanisms. This result further supports the use of discrete tracking strategies since small positioning inaccuracies have a negligible impact on overall energy production.

3.5 | Geographic Evaluation of the Sensorless Solar Tracking System Under Latitude and Longitude Variations

Using the validated simulation model, we investigated several Algerian locations covering the latitude range of approximately 33.5°–37.3° (Figure 14).

The observed decrease in energy production with increasing latitude is consistent with the reduction in annual solar resource availability and changes in solar elevation angles.

Unlike latitude, longitude does not affect the amount of solar energy available at a given location (Figure 15). Instead, it shifts the timing of solar noon and, therefore, the occurrence of peak power production (Figure 16). The proposed tracking strategy successfully compensates for this temporal shift through its astronomical positioning algorithm.

The limited variation among the investigated locations confirms that the proposed tracking strategy remains effective across Algeria's geographic extent.

3.6 | Cost Breakdown

Table 2 summarizes the cost of the developed prototype. The complete system costs approximately 307 USD (280 EUR), including the PV module, control hardware, actuation systems, and supporting structure. The stepper motors and PV module constitute the largest individual cost items, whereas the control electronics represent only a small fraction of the total investment.

The economic assessment indicates that the proposed prototype can be built with inexpensive, widely available components, resulting in a total system cost of approximately 307 USD. Although a direct cost comparison with commercial solar tracking systems is beyond the scope of this study, many

21944296, 2026, 11, Downloaded from https://onlinelibrary.wiley.com/doi/10.1002/ente.70709 by Ecole De Technologie Superieur, Wiley Online Library on [20/11/2026]. See the Terms and Conditions (https://onlinelibrary.wiley.com/terms-and-conditions) on Wiley Online Library for rules of use; OA articles are governed by the applicable Creative Commons License

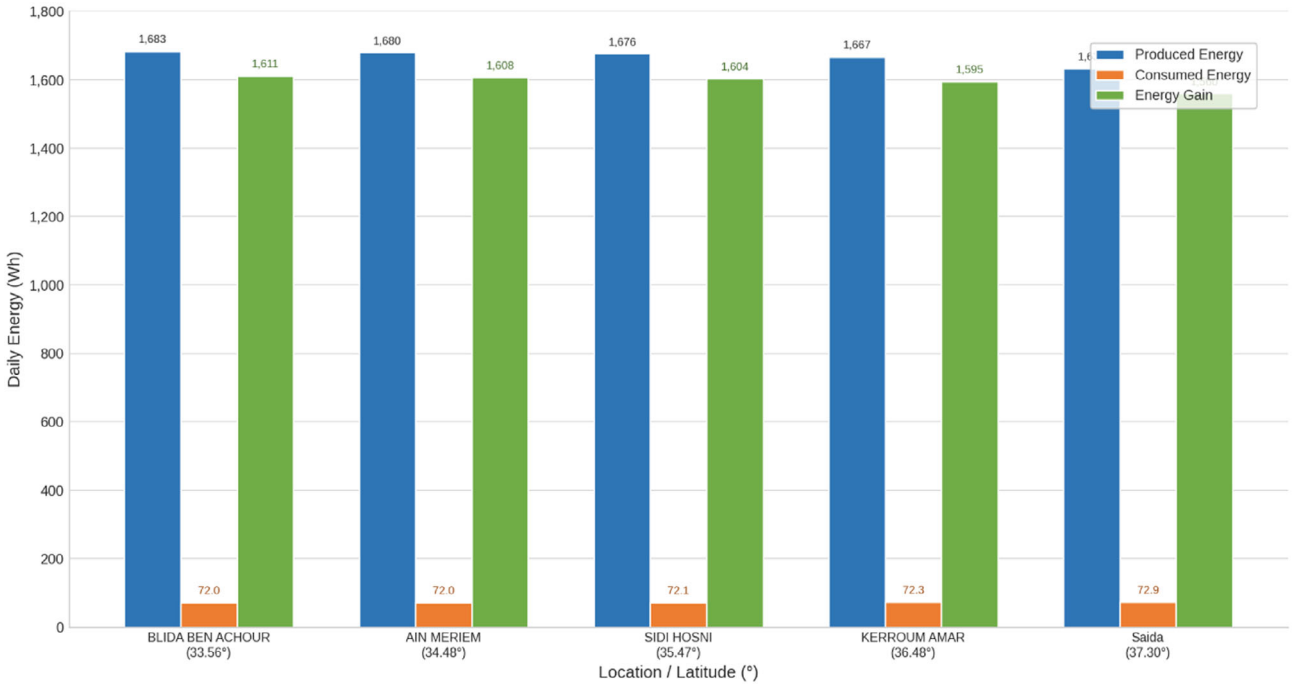


FIGURE 14 | Daily produced energy, tracker energy consumption, and net energy gain of the sensor-less solar tracking system for different latitudes in Algeria.

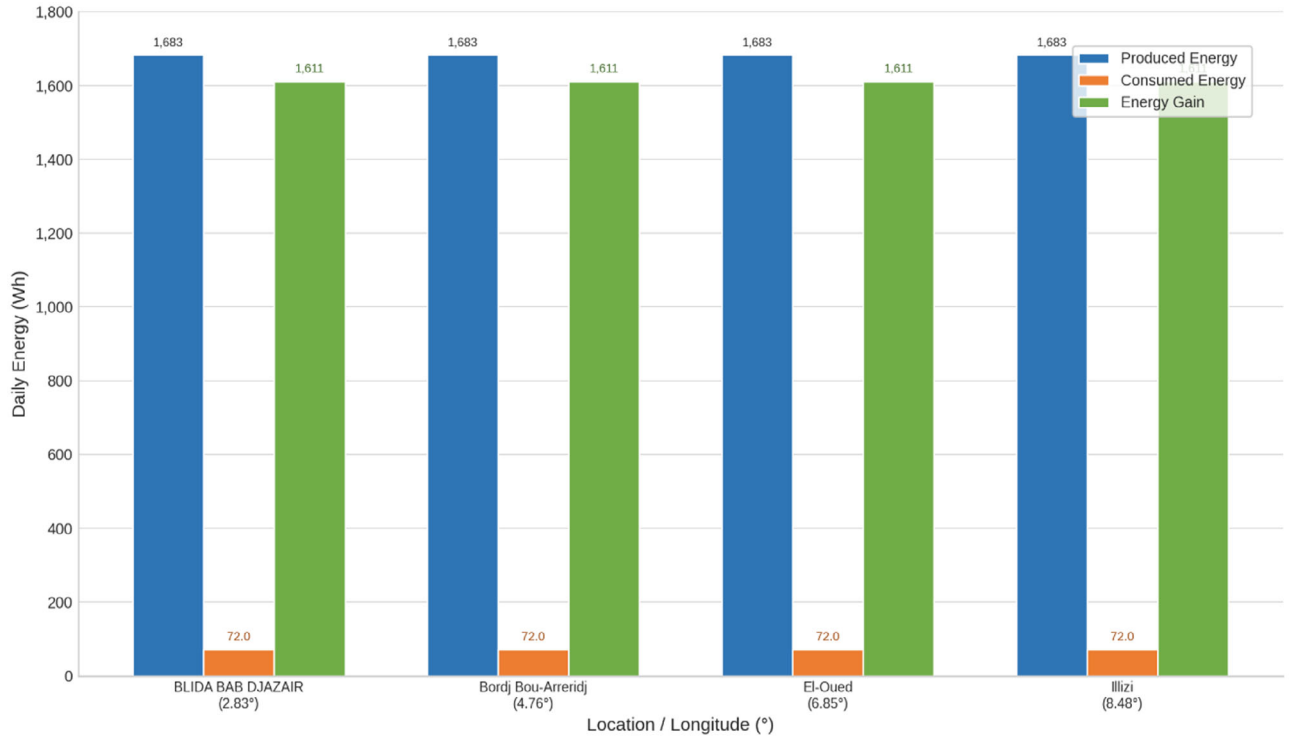


FIGURE 15 | Daily produced energy, tracker energy consumption, and net energy gain of the sensor-less solar tracking system for different longitudes in Algeria.

commercially available dual-axis trackers may rely on proprietary control units, dedicated sensors, GPS modules, or more complex mechanical assemblies, which generally increase acquisition and maintenance costs. By contrast, the proposed system employs a fully sensorless architecture based exclusively on astronomical calculations and geographic coordinates, thereby reducing hardware requirements and simplifying maintenance. These characteristics make the proposed design

21944296, 2026, 11, Downloaded from https://onlinelibrary.wiley.com/doi/10.1002/ente.70799 by Ecole De Technologie Superieur, Wiley Online Library on [20/11/2026]. See the Terms and Conditions (https://onlinelibrary.wiley.com/terms-and-conditions) on Wiley Online Library for rules of use; OA articles are governed by the applicable Creative Commons License

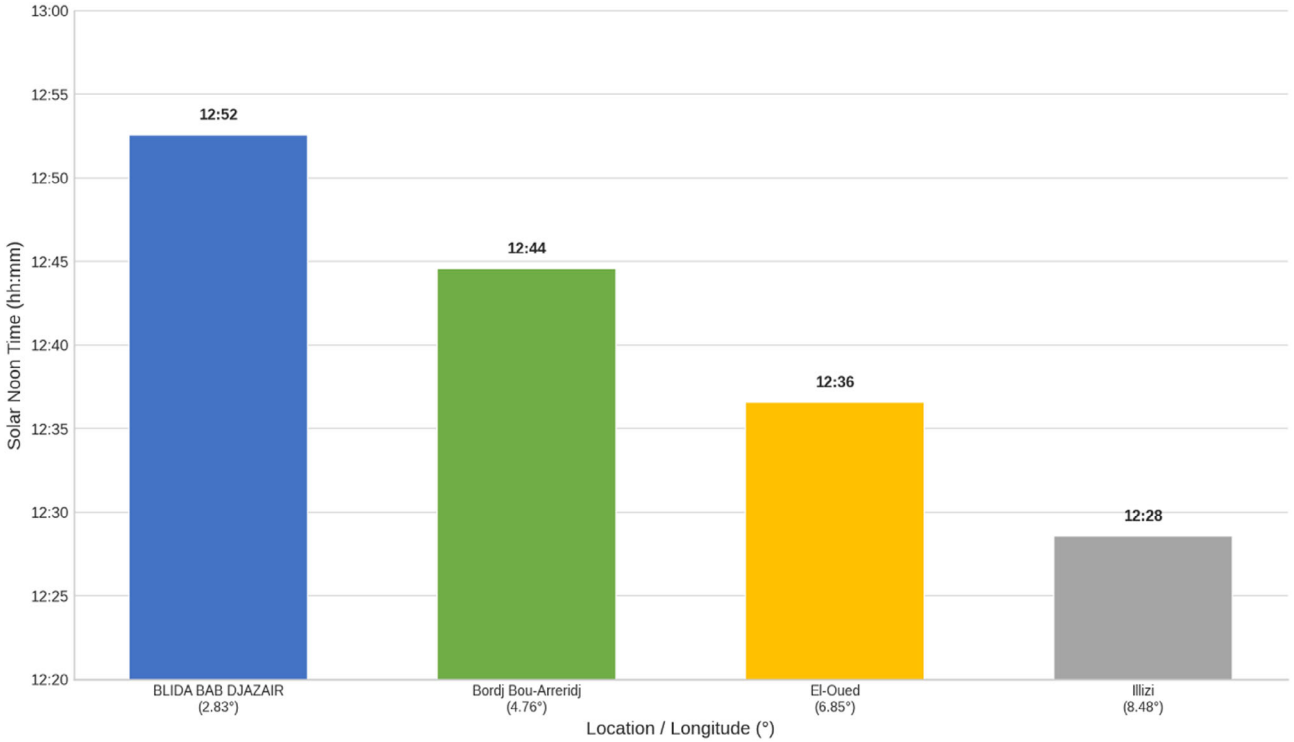


FIGURE 16 | Solar noon (time of maximum energy production) variation with longitude for different Algerian locations.

TABLE 2 | Cost breakdown for the implementation of the sensorless solar tracker components.

Category	Item	Quantity	Unit, DA	Cost, DA	Cost, USD	Cost, €
Control unit	Arduino mega	1	4832.02	4832.02	35.99	32.75
	L298N motor drivers	2	652.50	1305.01	4.86	4.42
	LCD I2C display	1	1196.26	1196.26	8.91	8.11
	3 × 4 keypad	1	965.33	965.33	7.19	6.54
Azimuth rotation system	V-belt	1	388.01	388.01	2.89	2.63
	Wooden pulley	2	537.04	1074.08	4.00	3.64
	NEMA 23 stepper	1	12 349.23	12 349.23	91.98	83.70
Elevation rotation system	Lead screw	1	1529.22	1529.22	11.39	10.36
	NEMA 17 stepper	1	2760.39	2760.39	20.56	18.71
Structural elements	Base with four wheels	1	1609.78	1609.78	11.99	10.91
	Support structure for solar panel	1	1342.60	1342.60	10.00	9.10
	Suntech STP050D-12/MEA solar panel	1	9343.15	9343.15	69.59	63.33
Power supply	12V power source	1	923.71	923.71	6.88	6.26
Others	Paint for structure coating	2	827.04	1654.08	6.16	5.61
	Resemblance cost	1	2000.47	2000.47	14.90	13.56
Total cost				43 273.34	307.29	279.63

particularly attractive for small-scale PV installations, educational applications, rural electrification projects, and deployments in resource-constrained regions, where affordability and reliability are critical considerations.

The low implementation cost, combined with the substantial energy gain from the tracker, suggests the additional investment could be recovered within a relatively short operating period, particularly in regions with high solar irradiance.

21944296, 2026, 11, Downloaded from https://onlinelibrary.wiley.com/doi/10.1002/ente.70799 by Ecole De Technologie Superieur, Wiley Online Library on [20/11/2026]. See the Terms and Conditions (https://onlinelibrary.wiley.com/terms-and-conditions) on Wiley Online Library for rules of use; OA articles are governed by the applicable Creative Commons License

3.7 | Comparison With Literature

To further assess the effectiveness of the proposed sensorless solar tracking strategy, we compared the results with representative solar tracking systems reported in the literature, including both sensor-based and sensorless approaches.

Previous studies have demonstrated that solar tracking systems can significantly improve PV energy production relative to fixed installations. Among sensor-based systems, Morón et al. [16] reported an 18% increase in energy output, while Hoffmann et al. [18] observed gains ranging from 17.2% to 31.1%. Sensorless approaches have also achieved substantial improvements, including up to 40% for the dual-axis tracker proposed by Tirmikci and Yavuz [23], 17.96% for the approach reported by Fuentes et al. [25], 20.1% for the particle-filter-based system developed by Pirayawaraporn et al. [26], and 35.91% for the dual-axis tracker proposed by Wu et al. [33]. More recently, Papadopoulos et al. [34] reported an annual average energy gain of 38.7% for a retrofitted sensorless dual-axis tracker operating under Mediterranean climatic conditions.

To further evaluate the proposed solar tracker's performance, Table 3 compares the developed system with representative sensor-based and sensorless tracking approaches reported in the literature. The comparison highlights each approach's tracking strategy, sensor requirements, reported energy gains, and principal limitations.

This energy gain was obtained using the validated simulation framework developed in this study, while the physical prototype was used to experimentally validate the tracking strategy and mechanical operation.

An important distinction among the systems reported in the literature concerns their dependance on sensing devices. Conventional sensor-based trackers typically employ photodiodes, webcams, or LDRs to determine the solar position [16–18]. Although these devices can provide accurate positioning, they increase hardware complexity and may require periodic calibration and maintenance. Furthermore, several systems described as sensorless still rely on auxiliary devices such as GPS receivers, digital compasses, pyranometers, current sensors, or MPPT-based feedback mechanisms [20, 21, 24, 25, 33]. By contrast, the proposed system relies exclusively on astronomical calculations and postal-code-derived geographic coordinates, eliminating the need for any dedicated sensing or positioning hardware.

The proposed ZIP-code-based sensorless tracker achieved a net energy gain of approximately 56.65% relative to a fixed PV panel. This value exceeds the gains reported in most representative sensor-based and sensorless systems listed in Table 3. The relatively high gain obtained in the present study can be attributed to the high solar resource available at the test location, the use of a dual-axis configuration, and the comparison against a fixed panel operated at a constant orientation. The results show that a fully open-loop architecture can achieve high tracking performance while maintaining minimal hardware requirements and low implementation costs.

A key advantage of the proposed approach is its simplicity. Several sensorless trackers reported in the literature still require additional hardware such as pyranometers, current sensors, GPS receivers, digital compasses, or maximum power point tracking units [20, 21, 24, 25]. In contrast, the proposed system relies exclusively on geographic coordinates derived from ZIP codes and astronomical calculations, resulting in a fully open-loop

TABLE 3 | Comparison of the proposed solar tracker with representative tracking systems reported in the literature.

Reference	Sensor-based	Tracking type	Reported energy gain	Main limitation	Key contribution
Morón et al. [16]	Yes	Dual-axis	18%	Requires photodiode sensors and periodic calibration	Low-cost Arduino-based implementation
Hoffmann et al. [18]	Yes	Dual-axis	17.2%–31.1%	Performance affected by weather conditions and LDR accuracy	Monthly energy performance assessment
Tirmikci and Yavuz [23]	No	Dual-axis	Up to 40%	Requires continuous mechanical tracking	Comparison between fixed and tracking systems
Fuentes et al. [25]	Partially	Dual-axis	17.96%	Requires current sensors and optimization routine	Current-based tracking optimization
Pirayawaraporn et al. [26]	No	Dual-axis	20.1%	Particle-filter algorithm increases computational complexity	Advanced estimation algorithm
Wu et al. [33]	Yes	Dual-axis	35.91%	Requires GPS, inclinometer, and compass sensors	High-accuracy tracking system
Present study	No	Dual-axis	56.65%	Electrical performance evaluated through validated simulations	ZIP-code-based sensorless tracking using astronomical calculations only

21944296, 2026, 11, Downloaded from https://onlinelibrary.wiley.com/doi/10.1002/ente.70709 by Ecole De Technologie Superieur, Wiley Online Library on [20/11/2026]. See the Terms and Conditions (https://onlinelibrary.wiley.com/terms-and-conditions) on Wiley Online Library for rules of use; OA articles are governed by the applicable Creative Commons License

architecture with reduced hardware complexity and maintenance requirements.

The analysis of tracking intervals further revealed that continuous tracking is not necessary to achieve high-energy performance. An hourly update interval provided near-optimal operation, while tracking intervals between 2 and 2.5 h maintained energy production above 99.8% while substantially reducing actuator energy consumption and mechanical activity. This finding contributes practical design guidance for future low-cost solar tracking systems.

The tracking-error analysis also demonstrated that deviations up to approximately 12° have only a limited impact on energy production. This result confirms observations reported in previous studies [31] and suggests that highly accurate positioning systems may not be economically justified for many PV applications.

The results indicate that the proposed ZIP-code-based tracker achieves one of the highest reported energy improvements while maintaining a completely sensorless architecture. Unlike many sensor-based systems that rely on optical sensors, cameras, or LDRs and several so-called sensorless systems that still require auxiliary devices such as GPS modules, compasses, current sensors, or pyranometers, the proposed approach relies exclusively on astronomical calculations and geographic coordinates. Furthermore, the achieved net energy gain of approximately 56.65% exceeds the gains reported in most comparable studies, demonstrating that high tracking performance can be obtained without increasing hardware complexity or maintenance requirements. The economic analysis further showed that the complete prototype can be implemented using commercially available components at relatively low cost. Combined with its robust performance under varying geographic conditions, this makes the proposed tracker particularly attractive for remote, rural, and resource-constrained regions, where affordability and reliability are critical considerations.

Overall, the proposed sensorless solar tracker combines high energy performance, low implementation cost, operational simplicity, and geographical adaptability, making it a competitive alternative to both conventional sensor-based trackers and more complex sensorless approaches reported in the literature.

4 | Conclusions

This study presented the design, implementation, experimental validation of the tracking mechanism, and simulation-based evaluation of the PV energy performance of a fully sensorless dual-axis PV solar tracking system based on astronomical ephemerides and ZIP-code–derived geographic coordinates. By eliminating the need for optical, irradiance, GPS, or positioning sensors, the proposed approach significantly reduces system complexity, maintenance requirements, and implementation costs while maintaining high tracking performance.

A comprehensive evaluation combining outdoor experimental validation of the tracking mechanism with simulation-based assessment of PV energy performance demonstrated the proposed strategy's effectiveness under varying operating conditions. The developed tracker achieved a net energy gain of approximately 56.65% relative to a fixed PV system, while the energy consumed by the tracking mechanism represented only 1.17% of the additional energy generated. These results confirm that a simple open-loop tracking architecture can substantially improve PV energy production.

The investigation further demonstrated that discrete tracking intervals are sufficient to maintain excellent performance. Although hourly tracking yielded the highest net energy gain, tracking intervals between 2 and 2.5 h provided an attractive compromise between energy production, actuator energy consumption, and mechanical wear. In addition, the system exhibited strong robustness to tracking inaccuracies, with angular deviations of up to 12° producing only minor reductions in energy output.

Geographic sensitivity analyses revealed that latitude primarily influences the magnitude of harvested solar energy, whereas longitude mainly affects the timing of peak solar production. The proposed tracking algorithm successfully accommodated both effects, confirming its suitability for deployment across a wide range of geographic locations.

The economic assessment showed that the complete prototype can be implemented with low-cost, commercially available components, making the proposed system particularly attractive for rural, remote, and developing regions where affordability and reliability are essential.

The principal contribution of this work lies in demonstrating that high-performance solar tracking can be achieved without sensors, complex optimization routines, or continuous actuation. The proposed ZIP-code-based tracking strategy provides a practical, scalable solution that improves PV energy production while keeping implementation and operating costs low.

Future work will extend the proposed framework by integrating artificial intelligence techniques for adaptive tracking optimization, weather-aware control strategies, predictive maintenance, and automated fault diagnosis. Additional investigations involving long-term field deployment in different climatic regions will further validate the robustness and scalability of the proposed sensorless solar tracking approach.

Acknowledgments

The authors would like to thank the L2GEGI Laboratory at Université IBN Khaldoun Tiaret for allowing us to perform the experiments and for providing the necessary support and facilities for the implementation of this work.

Funding

The authors have nothing to report.

Conflicts of Interest

The authors declare no conflicts of interest.

21944296, 2026, 11, Downloaded from https://onlinelibrary.wiley.com/doi/10.1002/ente.70709 by Ecole De Technologie Superieur, Wiley Online Library on [20/11/2026]. See the Terms and Conditions (https://onlinelibrary.wiley.com/terms-and-conditions) on Wiley Online Library for rules of use; OA articles are governed by the applicable Creative Commons License

Data Availability Statement

The data that support the findings of this study are available from the corresponding author upon reasonable request.

References

1. U. Gangopadhyay, S. Jana, and S. Das, "State of Art of Solar Photovoltaic Technology," in Conference Papers in Energy, vol. 2013 (Hindawi Limited, 2013), 1–9.

2. M. Dale and S. M. Benson, "Energy Balance of the Global Photovoltaic (PV) Industry—Is the PV Industry a Net Electricity Producer?," *Environmental Science & Technology* 47, no. 7 (2013): 3482–3489.

3. A. Jäger-Waldau, *Pv Status Report 2019* (Publications Office of the European Union, 2019).

4. SolarPower Europe, *Global Market Outlook for Solar Power 2020–2024, Technical Report* (SolarPower Europe, 2020).

5. SolarPower Europe, *Global Market Outlook for Solar Power 2022–2026, Technical Report* (SolarPower Europe, 2022).

6. International Energy Agency, *Renewables 2025: Analysis and Forecast to 2030, Technical Report* (IEA Publications, 2025).

7. J. Li, M. Chen, and P. Zhang, "Dominance and Diversification: An Analysis of China's Photovoltaic Industry in the Global Market, 2024," *Progress in Photovoltaics: Research and Applications* 32, no. 5 (2024): 567–582, https://doi.org/10.1002/pip.3780.

8. M. Hochberg, "*Algeria Charts a Path for Renewable Energy Sector Development* (Middle East Institute, 2020), https://www.mei.edu/publications/algeria-charts-path-renewable-energy-sector-development.

9. M. Benkhaled, M. T. Benmessaoud, and A. B. Stambouli, *High Penetration of Solar Energy to the Algerian Electricity System in the Context of an Energy Roadmap Toward a Sustainable Energy Paradigm by, 2030* (Springer, 2023).

10. E. Bellini, "Algeria's Sonelgaz launches 2 gw Solar Tender," February 2023, https://www.pv-magazine.com/2023/02/20/algerias-sonelgaz-launches-2-gw-solar-tender/.

11. V. Sumathi, R. Jayapragash, A. Bakshi, and P. K. Akella, "Solar Tracking Methods to Maximize Pv System Output—a Review of the Methods Adopted in Recent Decade," *Renewable and Sustainable Energy Reviews* 74 (2017): 130–138, https://doi.org/10.1016/j.rser.2016.11.190.

12. W. Nsengiyumva, S. G. Chen, L. Hu, and X. Chen, "Recent Advancements and Challenges in Solar Tracking Systems (sts): A Review," *Renewable and Sustainable Energy Reviews* 81 (2018): 231–279, https://doi.org/10.1016/j.rser.2017.07.061.

13. A. K. Sharma, R. Patel, and S. N. Singh, "A Global Performance Benchmark of Single-Axis and Dual-Axis Solar Tracking Systems: Meta-Analysis of Field Data From 2010-2023," *Renewable and Sustainable Energy Reviews* 189 (2024): 113987, https://doi.org/10.1016/j.rser.2023.113987.

14. N. Cheggaga, K. Dahli, M. R. Hammouda, A. Benallal, and A. Ilinca, "Innovative Shade Mitigation Technique for Maximizing Solar Energy Efficiency in Roof-Mounted Pv Systems," *Journal Européen Des Systèmes Automatisés* 57, no. 4 (2024): 1155–1164, https://doi.org/10.18280/jesa.570422.

15. L. Wang, H. J. Kim, and F. R. Gomez, "Dynamic Tracking Interval Control for Minimizing Actuation Losses in Photovoltaic Solar Trackers," *Energy Conversion and Management* 307 (2024): 118345, https://doi.org/10.1016/j.enconman.2024.118345.

16. C. Morón, D. Ferrández, P. Saiz, G. Vega, and J. P. Díaz, "New Prototype of Photovoltaic Solar Tracker Based on Arduino," *Energies* 10, no. 9 (2017): 1298, https://doi.org/10.3390/en10091298.

17. P. Garcia and M. Alejandro, "High-Precision Solar Tracking System," in World Congress on Engineering 2010, London, United Kingdom, 2010.

18. F. M. Hoffmann, R. F. Molz, J. V. Kothe, E. O. B. Nara, and L. P. C. Tedesco, "Monthly Profile Analysis Based on a Two-Axis Solar Tracker Proposal for Photovoltaic Panels," *Renewable Energy* 115 (2018): 501–759, https://doi.org/10.1016/j.renene.2017.08.057.

19. M. Abouzeid, "Use of a Reluctance Stepper Motor for Solar Tracking Based on a Programmable Logic Array (PLA) Controller," *Renewable Energy* 23, no. 3–4 (2001): 551–560, https://doi.org/10.1016/S0960-1481(00)00140-0.

20. M. H. M. Sidek, N. Azis, W. Z. W. Hasan, M. Z. A. A. Kadir, S. Shafie, and M. A. M. Radzi, "Automated Positioning Dual-Axis Solar Tracking System With Precision Elevation and Azimuth Angle Control," *Energy* 124 (2017): 46–170, https://doi.org/10.1016/j.energy.2017.02.047.

21. S. Seme and G. Štumberger, "A Novel Prediction Algorithm for Solar Angles Using Solar Radiation and Differential Evolution for Dual-Axis Sun Tracking Purposes," *Solar Energy* 85, no. 11 (2011): 2757–2770, https://doi.org/10.1016/j.solener.2011.08.031.

22. R. Nazir and M. Hadi, "Improve Dual Axis Solar Tracker Algorithm Based on Sunrise and Sunset Position," *Journal of Electrical Systems* 11, no. 4 (2015): 397–406.

23. C. A. Tirmikci and C. Yavuz, "Comparison of Solar Trackers and Application of a Sensorless Dual-Axis Solar Tracker," *Journal of Energy and Power Engineering* 9, no. 6 (2015): 556–561, https://doi.org/10.17265/1934-8975/2015.06.005.

24. H. Fathabadi, "Novel High Accurate Sensorless Dual-Axis Solar Tracking System Controlled by Maximum Power Point Tracking Unit of Photovoltaic Systems," *Applied Energy* 173 (2016): 448–459, https://doi.org/10.1016/j.apenergy.2016.04.020.

25. R. F. Fuentes-Morales, A. Díaz-Ponce, M. I. Peña-Cruz, et al., "Control Algorithms Applied to Active Solar Tracking Systems: A Review," *Solar Energy* 212 (2020): 203–219, https://doi.org/10.1016/j.solener.2020.10.045.

26. A. Pirayawaraporn, S. Sappaniran, S. Nooraksa, C. Prommai, N. Chindakham, and C. Jamroen, "Innovative Sensorless Dual-Axis Solar Tracking System Using Particle Filter," *Applied Energy* 338 (2023): 120946, https://doi.org/10.1016/j.apenergy.2023.120946.

27. K. Dahli, A. Ilinca, A. Benallal, and A. Tayeb, "Flocking-Inspired Solar Tracking System With Adaptive Performance in Varied Environmental Conditions," *Energies* 18, no. 8 (2025): 1967, https://doi.org/10.3390/en18081967.

28. T. Nguyen, V. K. Bhalla, and J. P. Correa, "Machine Learning for Sun Position Prediction in Sensorless Solar Tracking: A Review and Performance Comparison," *Engineering Applications of Artificial Intelligence* 133 (2024): 108112, https://doi.org/10.1016/j.engappai.2024.108112.

29. J. Canada-Bago, J. A. Fernandez-Prieto, M. A. Gadeo-Martos, and P. Perez-Higueras, "Knowledge-Based Sensors for Controlling a High-Concentration Photovoltaic Tracker," *Sensors* 20, no. 5 (2020): 1315, https://doi.org/10.3390/s20051315.

30. K. Dahli, A. Ilinca, A. Benallal, and N. Cheggaga, "Investigating Optimal Tracking Intervals for Solar Tracking Systems to Enhance Efficiency and Performance," in 2024 IEEE International Conference on Artificial Intelligence & Green Energy (ICAIGE) (2024), 1–6, https://doi.org/10.1109/ICAIGE62696.2024.10776746.

31. H. Mousazadeh, A. Keyhani, A. Javadi, H. Mobli, K. Abrinia, and A. Sharifi, "A Review of Principle and Sun-Tracking Methods for Maximizing Solar Systems Output," *Renewable and Sustainable Energy Reviews* 13, no. 8 (2009): 1800–1818, https://doi.org/10.1016/j.rser.2009.01.022.

32. T. Khatib and W. Elmenreich, *Modeling of Photovoltaic Systems Using Matlab: Simplified Green Codes* (John Wiley & Sons, 2016).

33. C.-H. Wu, H.-C. Wang, and H.-Y. Chang, "Dual-Axis Solar Tracker With Satellite Compass and Inclinometer for Automatic Positioning and Tracking," *Energy for Sustainable Development* 66 (2022): 308–318, https://doi.org/10.1016/j.esd.2021.12.012.

21944296, 2026, 11, Downloaded from https://onlinelibrary.wiley.com/doi/10.1002/ente.70709 by Ecole De Technologie Superieur, Wiley Online Library on [20/11/2026]. See the Terms and Conditions (https://onlinelibrary.wiley.com/terms-and-conditions) on Wiley Online Library for rules of use; OA articles are governed by the applicable Creative Commons License

34. G. P. Papadopoulos, K. T. Karagiannidis, and E. G. Voumvoulakis, "Experimental Annual Performance Assessment of a Low-Cost, Retrofit Dual-Axis Solar Tracker in a Mediterranean Climate," *Energies* 17, no. 8 (2024): 1945, https://doi.org/10.3390/en17081945.

35. J. H. Meeus, *Astronomical Algorithms* (Willmann-Bell, 1991).

Appendix A

Sun Position Calculation Algorithms

The following equations were used to compute the sun's position in the sky. These equations are based on Jean Meeus' "Astronomical Algorithms" [35].

Julian Date

The Julian Date is calculated from the year Y, month M, and day D, while A and B are auxiliary terms used to account for the calendar conversion.

$$\mathrm{JD} = 365.25(Y + 4716) + 30.6001(M + 1) + D + B - 1524.5 \tag{A1}$$

$$A = \frac{Y}{100}, \quad B = 2 - A + \frac{A}{4} \tag{A2}$$

Modified Julian Date and Julian Centuries

The modified Julian Date and Julian centuries T are derived from the Julian Date and provide the time scale required for the subsequent astronomical calculations.

$$+\mathrm{MJD} = \mathrm{JD} - 2\ 400\ 000.5, \quad T = \frac{(\mathrm{JD} - 2\ 451\ 545)}{36\ 525} \tag{A3}$$

Sun Position Parameters

The sun's mean longitude L_0, mean anomaly M, orbital eccentricity e, equation of the center C, true longitude θ, true anomaly v, and earth–sun distance R are calculated to determine the apparent solar position.

$$L_0 = 280.46646 + 36\ 000.76983T + 0.0001537T^2 \tag{A4}$$

$$M = 357.5291 + 35\ 999.0503T - 0.0001537T^2 \tag{A5}$$

$$e = 0.016708617 - 0.000042037T - 0.0000001267T^2 \tag{A6}$$

$$\begin{aligned} C = {} & (1.914602 - 0.004847T - 0.000014T^2)\sin(M) \\ & + (0.019993 - 0.000101T)\sin(2M) + 0.00029\sin(3M) \end{aligned} \tag{A7}$$

$$\theta = C + L_0 \tag{A8}$$

$$v = M + C \tag{A9}$$

$$R = \frac{1.000001018(1 - e^2)}{1 + e\cos(v)} \tag{A10}$$

$$\lambda = \theta - 0.00569 - 0.00478\sin(\Omega), \quad \Omega = 125.04 - 193.136T \tag{A11}$$

Obliquity, Right Ascension, and Declination

The apparent solar longitude λ is obtained by applying the correction associated with the sun's apparent motion, where Ω denotes the longitude of the ascending node of the moon's mean orbit.

$$\varepsilon = 23 + \frac{26}{60} + \frac{21.448}{3600} - \frac{46.815}{3600}T - \frac{0.00059}{3600}T^2 + \frac{0.001813}{3600}T^3 \tag{A12}$$

$$\tan(\alpha) = \frac{\cos(\varepsilon)\sin(\theta)}{\cos(\theta)} \tag{A13}$$

$$\sin(\delta) = \sin(\varepsilon)\sin(\theta) \tag{A14}$$

Hour Angles and Sun Position Angles

The Greenwich hour angle ω_G is calculated from the Julian Date and is combined with the geographic longitude λ and right ascension α to obtain the solar hour angle ω. The geographic latitude Φ, retrieved together with the longitude from the postal-code database, is then used with the solar declination δ and hour angle ω to calculate the solar elevation θ_{elev} and azimuth γ.

$$\begin{aligned} \omega_G = {} & 280.46061837 + 360.98564736629(\mathrm{JD} - 2\ 451\ 545) \\ & + 0.000387933T^2 - \frac{T^3}{38\ 710\ 000} \end{aligned} \tag{A15}$$

$$\omega = GHA + \theta - \alpha \tag{A16}$$

$$\sin(\theta_{\mathrm{elev}}) = \sin(\Phi)\sin(\delta) + \cos(\Phi)\cos(\delta)\cos(\omega) \tag{A17}$$

$$\tan(\gamma) = \frac{\sin(\omega)}{\cos(\omega)\sin(\Phi) - \tan(\delta)\cos(\Phi)} \tag{A18}$$

Appendix B

ZIP Code Table

See Table A1.

TABLE A1 | Geographic coordinates data for various postal codes in Algeria.

Postal code	Address	Latitude, °	Longitude, °
1000	Adrar	27.88	−0.29
44000	Ain–Defla	36.26	1.96
46000	Ain–Temouchent	35.30	−1.14
14039	AIN BEIDA	35.80	7.39
14040	AIN BOUCHEKIF	35.36	1.51
14007	AIN DEHEB	34.85	1.55
14017	AIN DZARIT	35.35	1.67
14008	AIN EL HADID	35.06	0.89
14009	AIN KERMES	34.91	1.11
14041	AIN MERIEM	37.30	9.87
14042	AIN RADJAH	36.17	1.05
9004	BLIDA BAB DJAZAIR	36.47	2.83
9026	BLIDA BEN ACHOUR	36.48	2.86
9016	BLIDA BEN BOULAID	36.49	2.83
14031	TIARET BOUHENNI	35.37	1.32
14000	TIARET RP	35.37	1.32
14035	TIARET UNIVERSITE	35.37	1.32

21944296, 2026, 11, Downloaded from https://onlinelibrary.wiley.com/doi/10.1002/ente.70709 by Ecole De Technologie Superieur, Wiley Online Library on [20/11/2026]. See the Terms and Conditions (https://onlinelibrary.wiley.com/terms-and-conditions) on Wiley Online Library for rules of use; OA articles are governed by the applicable Creative Commons License